Title	Enhancing reductive C-N coupling of nitrocompounds through interfacial engineering of MoO_2 in thin carbon layers
Author(s)	Mengting Liu, Xuexue Dong, Xiu Zhong, Zhenxiao Wang, Juanjuan Gong, Heng Song, Chao Yu, Aihua Yuan, Fu Yang and Edison Ang Huixiang

Enhancing reductive C-N coupling of nitrocompounds through interfacial engineering of MoO_2 in thin carbon layers

Mengting Liu,[a,#] Xuexue Dong,[a,#] Xiu Zhong,[a] Zhenxiao Wang,[a] Juanjuan Gong,[a] Heng Song,[a] Chao Yu,[a] Aihua Yuan,[a] Fu Yang,*[a] Edison Ang Huixiang*[b]

In this study, we developed an approach by coating silica nanospheres with polydopamine and metal precursor, followed by carbonization to create interfacial engineered MoO_2. The presence of numerous crystal interfaces and metal-carbon interactions resulted in a remarkable enhancement of C-N coupling activity and stability of catalyst compared to one obtained by air calcination.

As a prevalent category of essential chemicals, secondary amine compounds have extensive utilization in various industries, such as medicine, pesticides, cosmetics, rubber, and numerous other fields.[1a-e] As functional organic cooperatives continue to evolve, the demand for catalyst ligands, sensitivity materials, and antioxidants is experiencing rapid growth.[2] Currently, the C-N bond construction from nitrocompounds holds significant importance due to its ability to avoid the need for an additional reduction intermediate process, which is typically required to convert nitrocompounds into amino compounds.[3] Of greater significance, the reductive C-N coupling process is driven by its high synthetic selectivity and promising environmental friendliness, which contribute to its ongoing development. Particularly noteworthy is the adoption of cost-effective transition metal catalysts, replacing precious metal catalysts, which has garnered special attention in this regard.[4]

Heterogeneous Mo-based catalysts have been proven to exhibit activity in facilitating the formation of C-N bonds using nitrocompounds and boric compounds in the presence of specific reductants.[5] Notably, various studies have emphasized that the dimensions and atomic coordination structure of the Mo catalyst significantly impact the activity of C-N bond formation.[6] As an example, a previous study delved into the influence of electronic structure control of the Mo sites on the MoS_2 inert base via low-temperature modification. Additional control experiments and density theory calculations underscored that the introduction of oxygen at the interval site (Mo-S-Mo-O) enhances the adsorption and activation of the nitrocompound.[7] Furthermore, augmenting the Mo catalyst with an increased number of edge active sites results in a favorable enhancement of activity advantage.[8] This insight has inspired us to modify the coordination environment of the subsurface atom layer for Mo oxides. Additionally, the creation of abundant interfacial behavior in nanograins may facilitate the generation of more interfacial reaction regions, considering the active surface area. Drawing from these ideas, our study focuses on the in-situ liquid-phase polymerization, coating, and carbonization of polydopamine in conjunction with Mo atoms on the surface of SiO_2 to produce a thin-carbon layer confined interface engineering MoO_2 nanograins. These nanograins are utilized for the reductive C-N coupling reaction to construct secondary amines. Fig. 1a illustrates the detailed synthetic procedure employed for Mo/C@SiO_2. Specifically, at room temperature, SiO_2 nanospheres were utilized as internal core templates and dopamine hydrochloride incorporated with molybdenum phosphate was polymerized and self-assembled on the silica nanospheres, yielding the as-synthesized Mo/C@SiO_2 precursor. Subsequently, through a thermal carbonization process, the polydopamine (PDA) layer was transformed into a thin carbon layer coating on the silica core, while the Mo precursor decomposed into MoO_2 nanograins, confined within the carbon layer over silica core.

To assess the functional effect of the carbon layer and the unique modification of MoO_2 induced by PDA on the silica surface, several control sets were conducted. Specifically, the as-synthesized Mo/C@SiO_2 precursor was calcined in air, resulting in $Mo_{0.8}$@SiO_2-O_2 to exclude the presence of the carbon layer. Additionally, other Mo precursors, including ammonium molybdate, molybdenyl acetylacetonate, and sodium molybdate, were employed in the polymerization process, labeled as MoAm/C@SiO_2, MoMa/C@SiO_2, and MoSm/C@SiO_2, respectively.

Further optimization was carried out for the Mo loading and thermal treatment temperature, leading to $Mo_{0.6}$/C@SiO_2, $Mo_{0.8}$/C@SiO_2-700, $Mo_{1.0}$/C@SiO_2, $Mo_{0.8}$/C@SiO_2-600, $Mo_{0.8}$/C@SiO_2-800, and $Mo_{0.8}$/C@SiO_2-900. In Fig. S1 and S2 (ESI†), scanning electron microscopy (SEM) images depict the effects of carbonization temperature and calcined atmosphere on the morphology of various comparative samples. Despite variations in the aforementioned synthetic factors, all the samples maintain a well-defined nanospherical morphology. transmission electron microscopy (TEM) results provide insight into the microscale structure of the $Mo_{0.8}$/C@SiO_2 series samples obtained at the controlled temperatures. Specifically, as the carbonization temperature increases, a certain amount of carbon is lost during the carbonization process, resulting in the exposure of more active MoO_2 species. Conversely, higher temperatures can cause the aggregation of MoO_2 nanograins, leading to reduced exposure of the catalytic substance.

With the increase in carbonization temperature, the protective and supporting effect of carbon diminishes significantly, causing nanoparticles to be exposed from the carbon layer and evenly distributed on the carbon surface. Furthermore, a further increase in carbonization temperature can lead to the agglomeration of small particle nanoclusters. Based on these observations, the optimal catalyst synthesis temperature was determined to be 700 ℃. On the other hand, it was also observed that samples calcined in an air atmosphere directly led to the fracture of SiO_2 nanospheres, indicating that the introduction of the carbon layer provides a protective effect on the morphology of the samples.

The SEM image of $Mo_{0.8}$/@SiO_2-700 exhibits a uniform nanosphere structure with an approximate size of 230 nm (Fig. 1b). High-resolution (HR) TEM analysis of $Mo_{0.8}$/C@SiO_2-700 reveals the presence of lattice fringes corresponding to (210) and (111) of MoO_2, showcasing abundant grain boundaries behaviour (Fig. 1c-d). Furthermore, elemental analysis provides further confirmation of the successful doping of the molybdenum source and the distribution of each element. Notably, Mo atoms are uniformly distributed in the carbon layer on the surface of SiO_2 spheres.

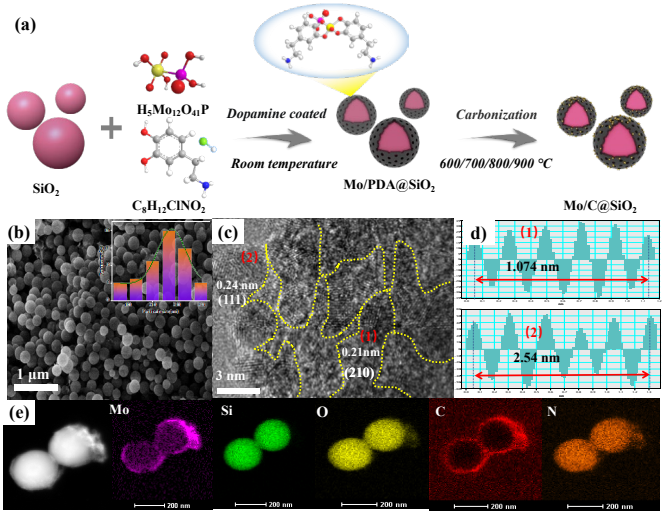

Fig. 1 (a) Synthetic description for Mo/C@SiO_2 nanosphere, (b) representative SEM images of $Mo_{0.8}$/C@SiO_2-700, (c) grain boundary evidence of nanospheres in the $Mo_{0.8}$/C@SiO_2-700 in HRTEM image and (d) the corresponding FFT and inverse FFT calculation of the selected regions, and (e) elemental mapping images of $Mo_{0.8}$/C@SiO_2-700.

A comprehensive characterization of the prepared samples was conducted using X-ray diffraction (XRD), Raman spectroscopy, and X-ray photoelectron spectroscopy (XPS). XRD characterization (Fig. S3, ESI†) revealed a more distinct diffraction peak pattern when phosphomolybdic acid was employed as the molybdenum source with an input amount of 0.8 mmol. Furthermore, Fig. S4 (ESI†) demonstrated that the crystalline phase of the prepared samples transformed from a pure MoO_2 phase to a mixed phase of MoO_2 and MoC with the gradual increase of the carbonization temperature. Considering that MoO_x is the primary active component in the C-N coupling reaction of nitroaromatics reduction, the calcination atmosphere was modified to air to promote the synthesis of MoO_x and investigate its effect on the C-N coupling reaction.[9] The results (Fig. 2a) indicated that the sample $Mo_{0.8}$@SiO_2-O_2 exhibited an amorphous state, suggesting that the introduction of the carbon layer facilitated the generation of MoO_2 nanocrystals.

Structural information of the catalyst was determined using Raman spectroscopy (Fig. S4, ESI†), and it was observed that the carbon defects decreased with the increase of Mo loading at the same carbonization temperature (Fig. S3c, ESI†). The presence of Mo is observed to effectively diminish carbon defects. Notably, when the loading capacity is 0.8 and the calcination temperature is set at 700 °C, a robust interaction between MoO_2 and carbon carriers occurs, facilitating favorable mutual electron transfer. Nitrogen adsorption-desorption and pore size distribution analyses (Fig. S5, ESI†) reveal an initial increasing and then decreasing relationship between the carbonization temperature and the specific surface area of the material. This phenomenon may be attributed to both the degree of carbonization and the aggregation of nanoparticles.[10] Similarly, the loading amount and specific surface area of the material exhibit a decreasing and then increasing relationship due to the partial blockage of pore size in SiO_2 by loaded nanoparticles. Subsequently, with further increases in loading amount, the nanoparticles on the surface of the nanospheres agglomerate and expose the apertures of SiO_2.[11] Additionally, it is noteworthy that the specific surface area of $Mo_{0.8}$/C@SiO_2-O_2, calcined under an oxygen atmosphere, experiences a significant reduction (5.06 m^2 g^{-1}) when compared to $Mo_{0.8}$/C@SiO_2-700, further reinforcing the significance of the carbon layer.

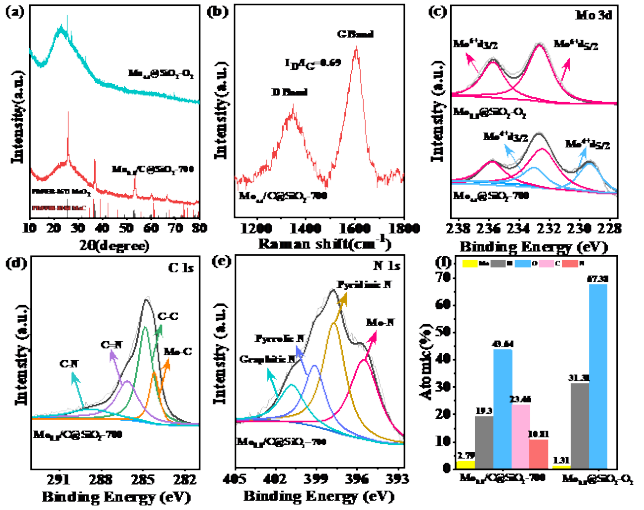

Fig. 2 (a) Wide-angle XRD patterns, (b) Raman spectra, (c-f) XPS spectra of $Mo_{0.8}$/C@SiO_2-700: (c) Mo 3d core level, (d)C 1s core level, (e) N 1s core level and (f) atomic ratio of the samples derived from XPS.

The activity of heterogeneous catalysts, particularly the role of abundant interfacial engineering, may be influenced significantly by the surface elemental states and coordination environment. These factors are crucial in determining the overall performance of the catalyst.[12] In this work, the effects of different carbonization temperatures and calcination atmospheres on the surface element states of the catalyst were further analysed by high-resolution XPS spectroscopy, which focused on the changes of surface elements as well as surface oxygen of the catalysts. Firstly, the XPS spectra of various comparison catalysts are shown in Fig. 2 and Fig. S6 (ESI†), where the catalysts are mainly composed of elements Mo, O, C, and N. All the Mo_{3d} peaks at 229.35 eV, 233.05 eV, 232.50 eV and 235.81 eV can be attributed to the $Mo_{3d}3/2$ and $Mo_{3d}5/2$ orbitals of Mo^{4+} and Mo^{6+}.[13] With the increase in carbonization temperature, the interaction between Mo and C atoms leads to changes in the electron cloud density, resulting in alterations in the binding energy of the Mo3d peak. Notably, $Mo_{0.8}$/C@SiO_2-700 exhibits a higher Mo^{4+} content, indicating a higher abundance of MoO_2. The peaks observed in C1s at 284.20 eV, 284.91 eV, 286.22 eV, and 287.80 eV correspond to Mo-C, C-C, C=N, and C-N bonds, respectively. The presence of C-Mo bonds suggests the incorporation of metal Mo, which consequently generates more active centers.[14, 15] In Fig. 2e, the peaks observed in N1s can be attributed to Mo-N, pyridine nitrogen, pyrrole nitrogen, and graphitic nitrogen from right to left, respectively. The existence of Mo-N bonding can enhance the catalytic activity of the catalyst by increasing its affinity to the reactant molecules.[16]

In heterogeneous catalytic reactions, the solution plays a crucial role. To assess the electron transfer ability of the catalyst under the influence of an electric field, electrochemical cyclic voltammetry (CV) was employed, as presented in Fig. S7 (ESI†). The outcomes demonstrate that $Mo_{0.8}$/C@SiO_2-700 exhibits the highest Cdl value of 1.16 mF cm^{-2}, indicating the greatest electron transfer capacity and electrochemically active surface area among the tested catalysts.[17, 18]

In this study, Mo/C@SiO_2 was employed as the catalyst for the coupling reaction, providing typical catalytic centers from the Mo sites and facilitating the transfer of active centers from inside the pores of SiO_2 to the outer surface. The coupling reaction involved the substrates chloronitrobenzene and p-

methoxyphenylboric acid, and optimal reaction conditions were achieved by controlling various variables (see Table S2, ESI†). Additionally, the influence of solvent polarity on the reactants was explored by altering the solvent. Notably, the highest yield of 94.3% for the secondary arylamine was achieved when toluene was used as the solvent under the optimum reaction conditions. Although higher yields could be obtained at a reaction temperature of 120 °C, 100 °C was chosen as the optimum experimental condition, considering economic benefits, and subsequent experiments were conducted under this reaction condition.

The performance of the synthesized series of comparative catalysts was investigated (Fig. 3a), highlighting the superiority of reasonable calcination temperatures and loading in the active build of Mo/C@SiO_2. Particularly, the active component Mo source exhibited a volcano-type variation between doping and yield, which can be attributed to excessive metal loading leading to the aggregation of highly dispersed nanoparticles and a reduction in the number of active centers.[19] Comparatively, $Mo_{0.8}$/C@SiO_2-700 showed enhanced reactivity when compared to $Mo_{0.8}$@SiO_2-O_2 obtained under an oxygen atmosphere. This result further supports the notion that the presence of the carbon layer promotes the formation of MoO_2 and enhances the active state of Mo. Additionally, in conjunction with the above characterizations, we suggest that the carbon skeleton and N doping play a role in accelerating the redox reaction by facilitating the electron transfer between the reactants and active species, thereby further enhancing the reaction yield.[20, 21]

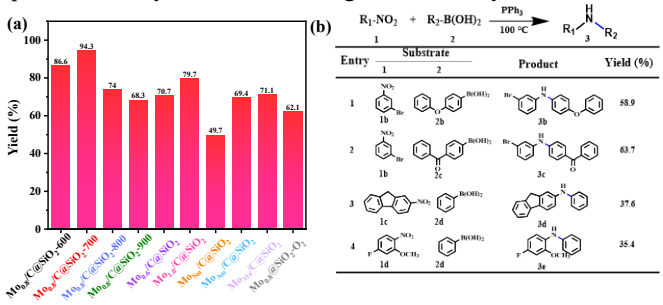

Fig. 3 (a) Yield of coupling 3a product over different catalysts. (b) The substrate scope used $Mo_{0.8}$@SiO_2-700 as the catalyst. Reaction conditions: reactants: 1b/c/d (0.2 mmol), 2b/c/d (0.3 mmol), using toluene as solvent (2 mL), under N_2 atmosphere at 100 °C for 24 h.

Subsequently, the optimal catalyst $Mo_{0.8}$/C@SiO_2-700 underwent specialized substrate expansion experiments to explore its broad reactivity range, as illustrated in Fig. 3b. Among these experiments, entries 1 and 2 focused on investigating the applicability of macromolecular boric acid substrates, while entries 3 and 4 examined the applicability to macromolecular nitro substrates with spatial site resistance effects. The results demonstrated that the coupling reactions with more complex nitro compounds and boronic acid compounds still exhibited good activity. In addition, the coupling suitability of the catalysts for aliphatic nitro compounds as well as aliphatic boronic acid compounds was considered. The results showed that the optimal catalysts exhibited good activity when employing aliphatic compounds (Table S3). Such above results indicate that the obtained catalyst affords wide flexibility in the various substrate scopes, which highlights the practical potential of catalyst in the industry. The effect of electron-withdrawing and electron-donating groups on the reactivity was further considered. 4-nitroethylbenzene was chosen as a control, and the results showed that the reactivity could be significantly promoted when electron-withdrawing substrates were present, while electron-donating substrates played the opposite role in the reaction process.

The lifetime and stability are key for heterogenerous catalysts.[22,23] To assess the stability of the heterogeneous catalyst, thermal filtration experiments were conducted. As depicted in Fig. S8 (ESI†), the reaction continued after the catalyst was filtered out, but the yield of 3a was found to be reduced by 18.8% at the end of the reaction, suggesting the possibility of Mo leaching during the reaction. ICP-OES analysis of $Mo_{0.8}$/C@SiO_2-700 before and after the reaction indicated a reduction in the Mo content by approximately 6 wt% after the reaction, implying the tendency of highly dispersed MoO_2 to undergo the exfoliation during the thermal reaction. Reusability and stability differences between $Mo_{0.8}$/C@SiO_2-700 and $Mo_{0.8}$@SiO_2-O_2 were explored through cyclic C-N coupling experiments. The results shown in Fig. S9 (ESI†) indicated that the yield of the optimal catalyst $Mo_{0.8}$/C@SiO_2-700 was 64.3% after four repetitions, which was about 30% lower than the initial yield but still significantly higher than that of the catalyst calcined in an oxygen atmosphere. This observation further validated the importance of the carbon layer for stabilizing the active MoO_2 species during the reaction process.

To further corroborate the above results, post-use characterization of the catalysts was conducted. Comparison of SEM images in Fig. S10 (ESI†) revealed no significant changes in morphology before and after the reaction. XRD results (Fig. S11, ESI†) indicated weaker diffraction peak intensities of used $Mo_{0.8}$/C@SiO_2-700, suggesting reduced crystallinity of MoO_2. Raman spectroscopy was employed to further analyze the carbon layer in the material, revealing significantly larger D-peaks associated with defects in the lattice structure of C atoms, suggesting the formation of numerous carbon defects during the reaction process, causing some C atoms in the carbon layer to break free from bonding and form defects. XPS analysis of the used catalysts $Mo_{0.8}$/C@SiO_2-700 (Fig. S12, ESI†) indicated a significantly lower content of Mo^{4+} after use, which might be a key factor contributing to the reduced activity. Fig. S12f (ESI†) presents the percentage of each element calculated according to XPS, demonstrating decreased Mo and C content and increased O content, possibly due to the adsorption of more oxygen after the formation of carbon defects during the reaction process.

In conclusion, we constructed interfacial engineered MoO_2 confined carbon layer over the SiO_2 nanosphere by polydopamine coatings and optimized the catalysts' active state by adjusting the heat treatment procedure and metal loading. The results demonstrated that the thermal decomposition of polydopamine in an inert atmosphere resulted in a thin carbon coating on the SiO_2 cores, while the formed MoO_2 exhibited ultrafine size and abundant interfacial effects. Additionally, it was observed that catalysts synthesized by calcination under an air atmosphere exhibited poor catalytic activity and stability, further underscoring the significance of the carbon layer in optimizing the active state of the MoO_2 active metal and improving the stability of active metal. This work presents a novel approach to the design of efficient molybdenum-based catalysts.

Financial support for this work was provided by the National Natural Science Foundation of China (21908085) and Natural Science Foundation of Jiangsu Province, China (BK20190961). We are appreciated of the support of characterizations from Instrumental Analysis Center, Jiangsu University of Science and Technology.

Notes and references

1 (a)A. Modak, A.J. Nett, E.C. Swift, et al., ACS. Catal., 2020, **10**, 10495-10499; (b) S. Suárez-Pantiga, R. Hernández-Ruiz, C. Virumbrales, et al., Angew. Chem., 2019, **58**, 2129-2133; (c) S. Das, F.D. Bobbink, G. Laurenczy, et al., Angew. Chem., 2014,

53 12876-12879; (d) T. Zhang, J. Vanderghinste, A. Guidetti, et al., Angew. Chem., 2022, **61**, e202212083; (e) A. Karakulina, A. Gopakumar, İ. Akçok, et al., Angew. Chem., 2016, **55**, 292-296.
2 P. Mäki-Arvela, I.L. Simakova, D.Y. Murzin, Catal. Rev., 2023, **65**, 501-568.
3 G. Li, Y. Kanda, S.Y. Hong, et al., J. Am. Chem. Soc., 2022, **144**, 8242-8248.
4 Y. Zhang, S. Ye, M. Gao, et al., ACS. Nano., 2022, **16**, 1142-1149.
5 W. Li, M. Huang, J. Liu, et al., ACS. Catal., 2021, **11**, 10377-10382.
6 D. Jiao, Y. Dong, X. Cui, et al., J. Mater. Chem. A., 2023, **11**, 232-240.
7 X. Dong, S. Yuan, M. Aizudin, et al., Appl. Surf. Sci., 2023, **624**, 157152.
8 K. Zhu, W. Qin, Y. Gan, et al., Chem. Eng. J., 2023, **470**, 144190.
9 F. Yang, X. Dong, Y. Shen, et al., ChemSusChem., 2021, **14**, 3413-3421.
10 S. Yang, W. Zhang, M. Liu, et al., J. Environ. Chem. Eng., 2023, **11**, 109190.
11 L. Cao, W. Liu, Q. Luo, et al., Nature, 2019, **565**, 631-635.
12 F. Yang, Y. Lu, X. Dong, et al., J. Hazard. Mater., 2020, **424**, 127647.
13 G. Yang, F. Feng, Y. Luo, et al., J. Environ. Chem. Eng., 2021, **9**, 106409.
14 X. Zhou, Y. Tian, J. Luo, et al., Adv. Funct. Mater., 2022, **32**, 2201518.
15 W. Wang, J. Qu, C. Li, et al., Mol. Catal., 2022, **532**, 112730.
16 Y. Wang, W. Cheng, P. Yuan, et al., Adv. Sci., 2021, **8**, 2102915.
17 Q. Song, M. Li, X. Hou, et al., Appl. Catal., B, 2022, **317**,121721.
18 Z. Feng, T. Ma, R. Li, et al., Mol. Catal., 2022, **530**, 112579.
19 C. Ranga, R. Lødeng, V.I. Alexiadis, et al., Chem. Eng. J., 2018, **335**, 120-132.
20 W. Han, L. Chen, B. Ma, et al., J. Mater. Chem. A., 2019, **7**, 4734-4743.
21 F. Wang, J. Jiang, K. Wang, et al., Appl. Catal., B, 2019, **242**, 150-160.
22 A. Jia, H. Zhang, J. Zhang, Mol. Catal., 2023, **549**, 113505.
23 A. Brik, M. E. Kadiri, T. E. Assimi, et al., Mol. Catal., 2023, **548**, 113422.